

***In vivo* imaging and characterization of hypoxia-induced neovascularization and tumor invasion**

GINA F. LUNGU¹, MENG-LIN LI², XUEYI XIE¹, LIHONG V. WANG² and GEORGE STOICA¹

¹Department of Pathobiology, College of Veterinary Medicine and ²Department of Biomedical Engineering, Optical Imaging Laboratory, Texas A&M University, College Station, TX, USA

Received June 6, 2006; Accepted July 12, 2006

Abstract. Hypoxia is a critical event in tumor progression and angiogenesis. Hypoxia can be detected noninvasively by a novel spectroscopic photoacoustic tomography technology (SPAT) and this finding is supported by our molecular biology investigation aimed to elucidate the etiopathogenesis of SPAT detected hypoxia and angiogenesis. The present study provides an integrated approach to define oxygen status (hypoxia) of intracranial tumor xenografts using spectroscopic photoacoustic tomography. Brain tumors can be identified based on their distorted vascular architecture and oxygen saturation (SO₂) images. Noninvasive *in vivo* tumor oxygenation imaging using SPAT is based on the spectroscopic absorption differences between oxyhemoglobin (O₂Hb) and deoxyhemoglobin (HHb). Sprague-Dawley rats inoculated intracranially with ENU1564, a carcinogen-induced rat mammary adenocarcinoma cell line, were imaged with SPAT three weeks post inoculation. Proteins important for tumor angiogenesis and invasion were detected in hypoxic brain foci identified by SPAT and were elevated compared with control brain. Immunohistochemistry, Western blotting, and semi-quantitative RT-PCR showed that HIF-1 α , VEGF-A, and VEGFR2 (Flk-1) protein and mRNA expression levels were significantly higher (P<0.05) in brain tumor tissues compared to normal brain. Gelatin zymography and RT-PCR demonstrated the upregulation of MMP-9 in tumor foci compared with brain control. Together these results suggest the critical role of hypoxia in driving tumor angiogenesis and invasion through upregulation of target genes important for these functions. Moreover this report validates our hypothesis that a novel noninvasive technology (SPAT) developed in our laboratory is suitable for detection of tumors, hypoxia, and angiogenesis.

Introduction

The oxygen status of tumors plays a central role in tumor pathophysiology and treatment. It is also a powerful prognostic factor of disease-free survival. In addition, it appears to be strongly associated with tumor growth, malignant progression, and resistance to various therapies including radiotherapy, photodynamic therapy, and chemotherapy (1). Prior studies involving different techniques have measured one or more parameters to define tumor hypoxia status. These include magnetic resonance imaging to monitor vascular oxygenation and blood flow (2), phosphorescence lifetime (quench) imaging (3) to measure oxygen diffusion distances between microvessels (4) and evaluate longitudinal tissue gradients of oxygen (5), cryospectrophotometry to measure hemoglobin saturation (6) single-photon emission computed tomography and positron-emission tomography assays to measure perfusion and mark hypoxic areas (7,8) and hypoxia markers to identify hypoxic tumor regions (9). Unfortunately, none of these technologies have produced a reliable measurement of tumor oxygen status and tumor vascularity primarily because solid tumors are usually characterized by a high degree of vascular and oxygen tension heterogeneity. The technique used in this study, spectroscopic photoacoustic tomography (SPAT) is based on the measurement of laser-induced ultrasonic waves and has contrast similar to that of pure optical imaging with spatial resolution similar to that of pure ultrasonic imaging. Therefore SPAT combines the advantages of two imaging modalities in a single modality. The laser-induced ultrasonic signals from biological samples depend on optical absorption in the sample to reveal the structure of the tissue based on optical contrast (10). The distribution of optical absorption in the object can be reconstructed using photoacoustic signals which are detected by highly sensitive piezoelectric devices. This technique used for detection of oxygen saturation (SO₂) is a noninvasive imaging modality, based on the spectroscopic differences between oxyhemoglobin (O₂Hb) and deoxyhemoglobin (HHb) (11). Since HHb and O₂Hb are the dominant absorbers in the rat brain region under study, with the reconstructed images at multiple optical wavelengths, the contributions to the photoacoustic signals from HHb and O₂Hb can be separated by SPAT; thus spatial distribution of total hemoglobin (HbT) and SO₂ based on the estimated concentration of HHb and O₂Hb can be reconstructed. SPAT has the ability to image HbT and SO₂ with satisfactory penetration depth in the rat brain.

Correspondence to: Professor George Stoica, Department of Pathobiology, Texas A&M University, College Station, TX 77843, USA

E-mail: gstoica@cvm.tamu.edu

Key words: HIF-1 α , hypoxia, MMP-9, spectroscopic photoacoustic tomography, VEGF, VEGFR2

Angiogenesis is an essential component for the growth of tumors. It is an invasive process that requires lyses of the extracellular matrix (ECM) plus proliferation and migration of the endothelial cells (12). This complex process, regulated by angiogenic factors and cytokines, is important for tumor invasion (13). Vascular endothelial growth factor (VEGF), an angiogenic mitogen secreted from various types of cells, is involved in various physiological and pathological conditions, including embryonic development, wound healing and solid tumor growth. VEGF is known to stimulate the production of various cytokines, growth factors, and proteinases, including MMP-1, -3, and -9 (14). The expression of VEGF is regulated by various physiological and pathological stimuli. Hypoxia is a strong inducer of VEGF, and hypoxia-induced VEGF expression determines the course of various disease conditions, such as solid tumor growth (15). Moreover, hypoxia has been shown to provide an important prognostic value in clinical trials involving radiation and chemotherapy. It is usually associated with adverse clinical outcomes and reduced patient survival (16). Although tissue hypoxia usually occurs very early in tumor development due to inadequate blood supply, hypoxia remains a constant feature of these tumors even after neovascularization (4). Several studies have shown that the regulation of gene expression by oxygen is an important feature of many biological processes, and hypoxia is a powerful modulator of gene expression (17,18). The main regulator which orchestrates the cellular responses to hypoxia is hypoxia-inducible factor-1 (HIF-1), a heterodimeric transcription factor composed of α and β subunits critical for adaptive responses to reduced oxygen (19). The HIF-1 β is thought to be expressed constitutively and ubiquitously. HIF-1 α is also constitutively expressed, but is continuously degraded in the presence of oxygen, by von Hippel Lindau tumor suppressor protein leading to decreased HIF levels in normoxia and high levels in hypoxia. Elevated HIF-1 α expression, which could be an indicator of the existence of hypoxia, has been reported in a variety of human tumors and pre-neoplastic lesions (20,21). The critical role of HIF-1 α in tumor metastasis arises from the fact that it is a potent activator of angiogenesis and invasion through its upregulation of target genes important for these functions. Hill and co-workers have found that exposure of tumor-bearing rodents to cyclical, but not chronic, hypoxia produces a significant increase in metastasis to the lungs (22). Hypoxia was also found to be important in activation of extracellular matrix degrading proteases (23).

Matrix metalloproteinases (MMPs) are structurally related endopeptidases that play a role in proteolytic degradation of structural components of extracellular matrix (24). They not only facilitate breakdown of extracellular matrix, but also affect early carcinogenesis, tumor development and growth. They also play an important role in angiogenesis and mammary gland involution (25). Among these enzymes, matrix metalloproteinase-9 (MMP-9) or gelatinase B plays an important role in tumor invasion and metastasis because of its specificity for type IV collagen. Recent studies have demonstrated that the switch from vascular quiescence to angiogenesis involves MMP-9/gelatinase B, which is upregulated in angiogenic islets and tumors, releasing VEGF from an extracellular reservoir (26). Prior observations have suggested that acidity in the tumors can be caused by hypoxia-dependent and/or independent

pathways and MMP-9 was found to be induced by culturing cells at acidic pH (27). Acidic pH was also found to increase the expression of vascular endothelial growth factor in glioma (28), and glioblastoma (29).

The present study provides an integrated approach to define the oxygen status (hypoxia) of tumors by using SPAT and to correlate hypoxia with the invasion process of a mammary adenocarcinoma cell line ENU1564 inoculated intracranially in a rat model. The mechanism of tumor invasion may apply to tumor metastasis because metastasis mediators are involved in both of these processes. Here we were able to successfully obtain the brain oxygenation images, which clearly showed tumor hypoxia. We also evaluated the expression of HIF-1 α , VEGF, VEGFR2 and MMP-9 protein and mRNA levels in the hypoxic brain tumor foci. We demonstrated that the levels of HIF-1 α , VEGF, VEGFR2 proteins in brain tumor foci were higher than the ones of normal brain tissues. Additionally, MMP-9 enzymatic activity was higher in brain tumor foci. The results were confirmed by semi-quantitative RT-PCR. The regulation of proteins targeted in our study may be directly correlated with hypoxia detected in the brain tumor foci by SPAT. Such informations can be used not only as a prognostic tool for tumor invasion but also as the basis for developing and evaluating patient-specific treatment modalities for many types of cancers. It should be possible to target hypoxic cells by developing a gene therapy strategy that uses plasmids containing suicide genes that are selectively expressed under hypoxic conditions.

Materials and methods

Reagents. Chemicals, stains and solutions were obtained from Sigma Chemical Co. (St. Louis, MO, USA) unless otherwise indicated.

Cell culture. The ENU1564 tumor cell line used in this study was originally developed in our laboratory and originated from an *N*-ethyl-*N* nitrosourea-induced mammary adenocarcinoma in a female Berlin-Druckrey IV (BD-IV) rat. This cell line is highly metastatic to brain and bone tissues (30). Prior to inoculation, the cell line was maintained in Dulbecco's modified Eagle's medium (DMEM) (Invitrogen, Carlsbad, CA, USA), supplemented with 10% fetal bovine serum (Invitrogen) and antibiotics (100 units/ml penicillin and 100 μ g/ml streptomycin).

Rat inoculation. Three-week old Sprague-Dawley (SD) rats obtained from a colony maintained at Texas A&M University were used. All animal experiments were done in accordance with protocol approved by our Institutional Animal Care and Use Committee (IACHC) and following National Institute of Health (NIH) guidelines for animal welfare. Stereotaxic implantation of tumor cells was performed under full anesthesia using a mixture of Ketamine (Ketant, Fact Dodge Animal Health) and xylazine (Ane Sed, Lloud Laboratories). A stereotaxic frame was used to stabilize the animal's head. The hair on the rat's head was gently removed with hair-removal lotion. The site of inoculation was marked at a point 2.5 mm lateral and 1 mm anterior to the bregma. This point was chosen because of its location directly above the caudate nucleus,

which has been shown to be a highly reliable intracranial site for tumor engraftment. The cells were inoculated intracranially at 3 mm depth from the cranial surface. A Hamilton syringe was used to inoculate 3 μ l tumor cell suspensions (5×10^6 cells) over 5 min period. Three weeks post inoculation the animals were subjected to SPAT evaluation. After the SPAT evaluation the animals were euthanized with Pentobarbital (150 mg/kg, intraperitoneal injection) and the brain tumors were used for Western blot analysis, gelatin zymography, and RT-PCR experiments.

Tissue processing and tumor collection. For Western blot analysis, gelatin zymography, and RT-PCR, brains were immediately removed after death and placed on powdered dry ice. Brains from rats inoculated intracranially with tumor cells (n=3) and from age-matched non-inoculated control rats (n=3) were used. Samples were kept at -80°C . Brain tumors were collected from frozen brain sections. The half of the brain that was frozen in powdered dry ice was sectioned using a cryostat (Bright Instrument Company, Ltd., Huntington, UK) in 12 μ m sections and placed on slides. Every fifth slide was stained with 0.1% thionine solution. Thionine solution stained the cell nuclei and displayed the tumor foci under light microscopy. The information was used to dissect the tumor foci, on frozen brain tissue sections. For immunohistochemistry, brain tumor-bearing (n=3) and tumor-free (n=3) SD rats were perfused with 4% paraformaldehyde (PFA) solution (Electron Microscopy Science, PA, USA) in PBS (phosphate buffer saline) using a peristaltic pump. Brains were then removed and post-fixed in 4% PFA in PBS for 24 h, after which the brains were further processed.

Immunohistochemistry. Five-micron paraffin-embedded sections were used for immunohistochemical study. After deparaffinization the sections were subjected to an antigen retrieval protocol by heating them in 10 mM citrate buffer (pH 6.0) for 10 min. Potential non-specific binding sites were blocked with 5% normal goat or rabbit serum in PBS. After blocking, the sections were incubated for 1 h to overnight with primary antibody. For activated microglial cells we used a mouse anti-rat CD68: biotin from Serotec Company (Hidlington, Oxford, UK). Mouse anti-gial fibrillary acidic protein (GFAP) was purchased from Chemicon International (Temecula, CA, USA). The other primary antibodies, MMP-9, VEGF-A, VEGFR2, and HIF-1 α were purchased from Santa Cruz Biotech (Santa Cruz, CA) and a 1:50 dilution was used. Following primary antibody reaction, sections were washed and incubated with either biotin-conjugated anti-rabbit or anti-goat IgG (Vector Laboratories, Burlingame, CA, USA). A Vector-ABC streptavidin-peroxidase kit with a benzidine substrate for color and streptavidin-phosphatase kit (KPL, MD, USA) with a HistoMark Red substrate (KPL) were used for color development. Counter-staining was done with diluted hematoxylin. Sections that were not incubated with primary antibody served as negative control. To visualize the tumor foci on paraffin-embedded sections, hematoxylin and eosin staining was performed.

Western blot analysis. After microscopic dissection of frozen brain specimens, the tissues was homogenized in lyses buffer

containing 50 mM Tris-HCl (pH 7.4), 150 mM NaCl, 1 mM CaCl_2 , 1 mM MgCl_2 , 0.1% Triton X-100. The lysates were cleared by centrifugation at $13,000 \times g$ at 4°C for 30 min, and the supernatant kept frozen at 80°C . The protein content of the lysates was determined using Bradford Assay (Bio-Rad), with bovine serum albumin as the standard. Proteins (15-30 μ g) were separated by 9-12% SDS polyacrylamide gel electrophoresis (SDS-PAGE) and transferred to nitrocellulose membranes (Schleicher and Schuell, Keene, NH, USA). Membranes were incubated 1 h in blocking buffer (20 mM Tris-HCl buffered saline containing 5% nonfat milk powder and 0.1% Tween-20) at room temperature and then probed with appropriate antibodies in blocking buffer or blocking buffer including 5% bovine serum albumin instead of 5% nonfat milk overnight at 4°C . Blots were incubated at 4°C overnight with anti-MMP-9 (1:200); anti-HIF-1 α (1:200), anti-VEGF-A (1:200), anti-VEGFR2 (Flk-1) (1:100), (all antibodies from Santa Cruz Biotech), washed extensively and then incubated for 1 h with a 1:5000 dilution of secondary antibody. Peroxidase labeled anti-rabbit and anti-mouse secondary antibody were purchased from Kirkegaard and Perry Laboratories (MD, USA). Monoclonal mouse IgG antibody against β -actin was purchased from Sigma Chemical Co. After additional washes, the blots were incubated with chemiluminescent substrate, according to directions in the kit (Super Signal West Pico, Pierce, Rockford, IL).

Gelatin zymography. Gelatinolytic activities were analyzed by gelatin zymography as previously described (31). Protein lysates were incubated at 37°C for 30 min in SDS sample buffer without reducing agent and then subjected to SDS-PAGE in 10% (wt/vol) polyacrylamide gels containing 0.1% (wt/vol) gelatin. The gels were washed twice for 30 min in 2.5% (vol/vol) Triton X-100 at room temperature and then incubated for 24 h in substrate reaction buffer [50 mM Tris-HCl (pH 7.5), 100 mM NaCl, 10 mM CaCl_2 , 0.002% NaN_3] at 37°C . The gels were then stained with Coomassie Brilliant Blue R250 in 10% (vol/vol) acetic acid and 30% (vol/vol) methanol for 1 h and destained briefly in the same solution without dye. Proteolytic activities were detected as clear bands indicating the lyses of the substrate.

Total RNA extraction and semi-quantitative RT-PCR. Total RNA was extracted from frozen specimens using an SV RNA extraction kit (Promega) following the manufacturer's directions. RNA was quantified by absorbance at 260 nm. Using a SuperScript III First Strand Synthesis System (Invitrogen), 100 ng of total RNA was amplified by reverse transcription polymerase chain reaction (RT-PCR) and the cDNAs were amplified in a 25- μ l reaction. PCR primers were as follows: MMP-9 primers (forward, 5'-CCCCACTTACTTTGGAAACGC-3'; reverse, 5'-ACCCACGACGATCAGATGCTG-3') (32); HIF-1 α primers (forward, 5'-GTCCGACAGCCTCACCAAACAGAGC-3'; reverse, 5'-GTAACTTGATCCAAAGCTCTGAG-3') (33); VEGF primers (forward, 5'-GACCCTGGTGGACATCTTCCAGGA-3'; reverse, 5'-GGTGAGAGGTCTAGTTCCCGA-3') (14); β -actin primers (forward, 5'-ATGTACGTAAGCCAGGC-3'; reverse, 5'-AAGGAAGTGGAAAAGAGC-3') (32).

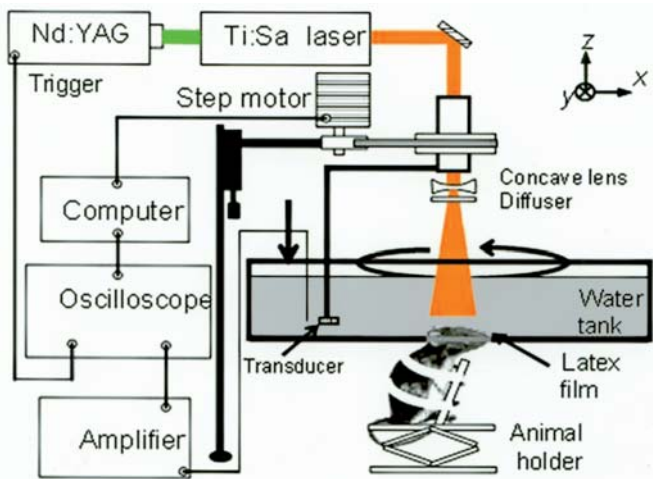


Figure 1. Experimental setup for the *in vivo* SPAT of an SD rat head.

The expected size for MMP-9 PCR product was 686 base pairs (bp). PCR condition for MMP-9 was carried out with an initial denaturation of 94°C for 2 min, followed by 30 cycles at a denaturation of 94°C for 1 min, annealing at 59.1°C for 30 sec and extension at 72°C for 1 min. A final extension of 5 min at 72°C was carried out. For HIF-1 α , 25 cycles were carried out with 30 sec at 95°C, 1 min at 55°C and 2.5 min at 72°C. A final extension of 7 min at 72°C was carried out. The PCR product size for HIF-1 α was 487 bp. For VEGF, one set of rat primers, which amplified 3 splicing variants of a rat VEGF mRNA (VEGF₁₂₀, VEGF₁₆₄ and VEGF₁₈₈) was used. The PCR profile consisted of initial denaturation at 94°C for 7 min, followed by 35 cycles of denaturation at 94°C for 30 sec, annealing at 58°C for 30 sec, extension at 72°C for 90 sec, and extension at 72°C for 7 min. The expected length of the PCR products was 330 bp for VEGF₁₂₀, 462 bp for VEGF₁₆₄, and 514 bp for VEGF₁₈₈. To demonstrate the integrity of the RNA samples used in the RT-PCR reactions, parallel amplifications with oligonucleotide primers for mouse β -actin were performed. The expected size for β -actin PCR product was 403 bp. PCR fragments were analyzed on 1.5% agarose gels stained with ethidium bromide.

Experimental setup of SPAT. Three weeks after intracranial inoculation, experimental rats had developed neurological signs such as ataxia and head tilt. At that time the experimental rats were imaged using SPAT. Four successful SPAT images showing tumor hypoxia in the SD rat brains were achieved as described in Fig. 1. Three rats of similar age, inoculated intracranially with 3 μ l of DMEM medium, were used as controls. Briefly, each animal was anesthetized using Ketamine (87 mg/kg, intramuscular injection) and the hair from the top of the head was removed. A tunable Ti:Sa nanosecond pulse laser (LT-2211A, Lotis T II, Minsk, Belarus) pumped by an Nd:YAG laser was employed to provide laser pulses with a pulse repetition rate of 10 Hz. The laser beam was expanded by a concave lens and homogenized by a light diffuser and then delivered to the animals head (Fig. 1). The incident energy density of the laser beam on the surface of the rat head was controlled at \sim 20 mJ/cm² (within the ANSI standard). The energy of each single laser pulse was monitored using a

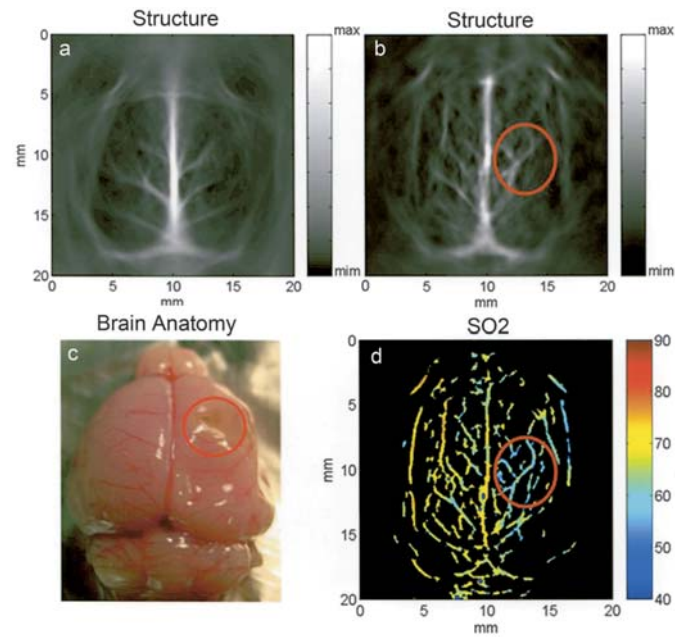


Figure 2. Estimated brain blood oxygen saturation image from noninvasive *in vivo* spectroscopic photoacoustic tomography (SPAT) of an SD rat brain at three weeks post inoculation with ENU1564 cells. The circle indicates the position of the tumor. (a), SPAT image of a tumor-free rat brain, which shows well-defined symmetrical vascular architecture in both cerebral hemispheres. (b), SPAT image of the rat brain inoculated intracranially with ENU1564 cells and reveals the vascular architecture associated with the tumor, which is different from that of a normal brain SPAT image. (c), Open-skull photograph of the rat brain after SPAT experiment shows the tumor position in the cerebral hemisphere. (d), Estimated brain blood oxygen saturation (SO₂) image.

photodiode (PD) and recorded. The photoacoustic signals were normalized by the recorded PD signals to reduce the effect of laser-energy fluctuation. A 2.25-MHz ultrasonic transducer (V323, Panametrics) was used to detect the laser-induced acoustic signals. The active area diameter was 6 mm and it had a nominal band-width of 66%. A computer controlled step motor drove the 2.25 MHz transducer to circularly scan the head of the SD rat at a depth of \sim 3 mm below the skin surface, at a radius of 4.5 cm, and with a step size of 3 degree. During the SPAT scan, the rat was fixed by a homemade restraint mount. A water tank was used that had a sealed opening in the bottom such that the rat's head could protrude along the bottom of the water surface and stay dry (Fig. 1). The hole was sealed with a piece of polyethylene membrane. The rat head surface was covered with a thin layer of ultrasonic coupling gel. Health status, pulse rate and the global arterial blood oxygenation of the rat were monitored throughout the entire experiment using a pulse oximeter. The detected photoacoustic signals were amplified, digitized by an oscilloscope, and then transferred to a computer. Four wavelengths (764, 784, 804, and 824 nm) were changed at each scanning step. After a single full-view scan, the images at different wavelengths were reconstructed based on a modified back projection algorithm (34). Then the reconstructed images at the four different wavelengths were used to estimate the spatial distribution of the concentration of HHb and O₂Hb using a standard linear least-squares method.

Statistical analysis. Quantification of the Western blot analysis, gelatin zymography, and semi-quantitative RT-PCR bands

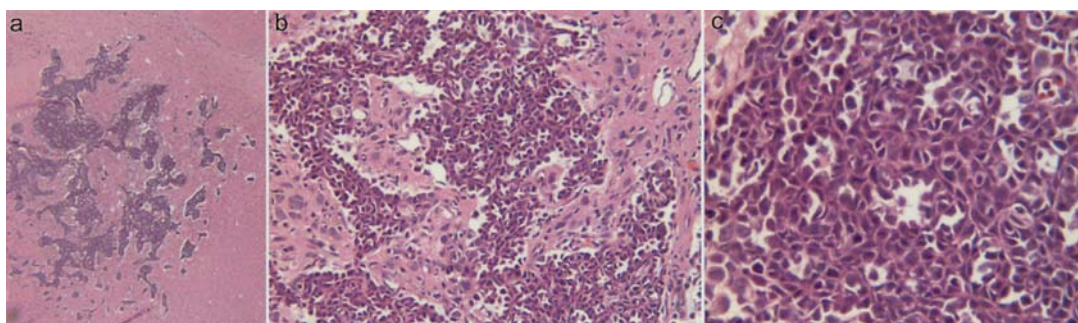


Figure 3. Histology (H&E staining) of the tumor foci inside the SD rat brain at various microscopic magnifications (a-c). The tumor is observed as a basophilic, hypercellular area composed of neoplastic epithelial cells. (a), x4; (b), x20; and (c), x40.

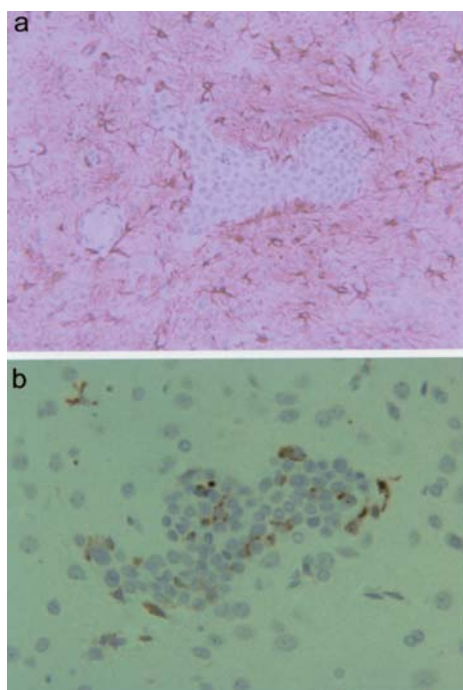


Figure 4. Activation of astrocytes and microglial cells around and inside the brain tumor foci. (a), Activation of astrocytes (brown color) around tumor foci (immunohistochemical staining for GFAP) (x10). No reactivity of astrocytes was observed inside the brain tumor foci. (b), Active microglial cells around and inside the tumor foci, which is denoted by brown color (x20). Arrows indicate the tumor foci.

density was performed on a Macintosh computer using the public domain NIH Image program (developed at the US National Institutes of Health and available on the internet at <http://rsb.info.nih.gov/nih-image>). Data were presented as mean \pm SD, and statistical comparisons were made using Student's t-test. A P-value of <0.05 was considered statistically significant.

Results

Spectroscopic photoacoustic tomography (SPAT) imaging of the SD rat brain tumor three weeks after inoculation with ENU1564 cell line. SPAT images from four tumor-bearing SD rat brains showed hypoxia. The most representative SPAT image of brain tumor hypoxia is showed in Fig. 2. None of

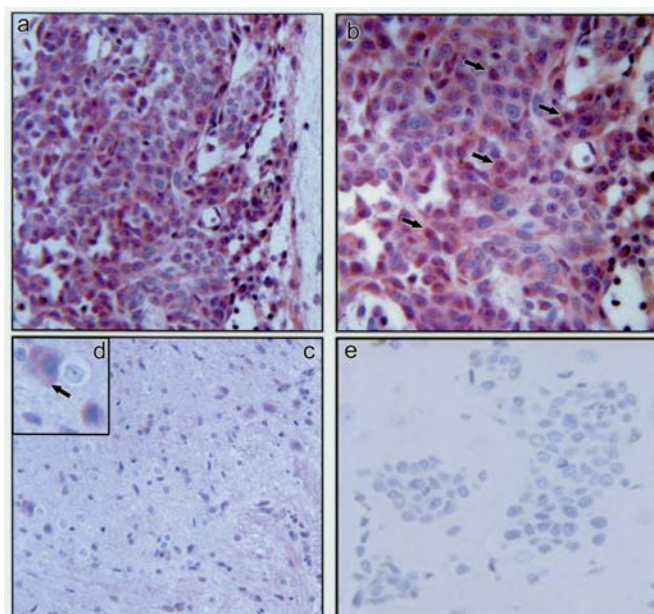


Figure 5. Localization of HIF-1 α in hypoxic tumor foci. Immunohistochemical staining (red) of HIF-1 α protein in the tumor foci revealed positivity within neoplastic cell cytoplasm and nucleus (a and b) (x10). Arrows indicate the neoplastic cells within tumor foci which stain positive for HIF-1 α in both cytoplasm and nucleus. Positive control is represented in (c) and revealed cytoplasmic HIF-1 α staining (x10). (d), Higher magnification view of the neurons in (c). Note the absence of nuclear HIF-1 α staining in neurons. Arrow indicates cytoplasmic HIF-1 α staining of the neurons. Sections exposed to a negative control antibody showed no staining reactions (e). (x20).

the SPAT images of tumor-free SD rat control brains showed hypoxia. Differences in brain vasculature between a tumor-free SD rat brain (Fig. 2a) and a tumor-bearing SD rat brain (Fig. 2b) are illustrated. Compared with the tumor-bearing rat brain, SPAT images of the tumor-free brain showed a well-defined symmetrical vascular architecture in both cerebral hemispheres. In Fig. 2c, an open-skull photograph of the rat brain taken right after the SPAT experiment, showed a tumor in the right hemisphere. The position of the tumor corresponded with the location of the tortuous irregular distorted vessels shown in Fig. 2c. The SO₂ image of the rat brain with intracranial inoculation of ENU1564 cells is represented in Fig. 2d. The SO₂ value is lower in the brain tumor area compared to the rest of the brain. Fig. 3 shows the H&E staining of the tumor foci inside the rat brain imaged by SPAT. The diameter

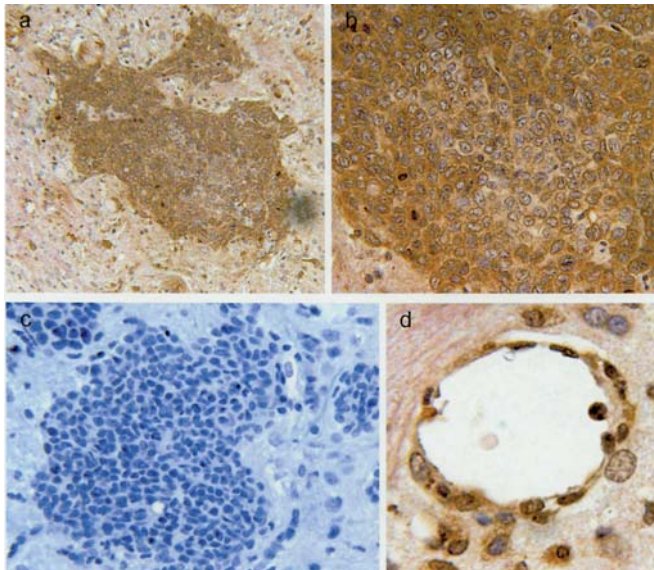


Figure 6. Localization of VEGFR2 (Flk-1) in tumor foci. (a), VEGFR2 labeling of the tumor foci (x10). (b), Higher magnification view of tumor cells showing cytoplasmic and membrane VEGFR2 staining (x20). (c), No staining was observed in the negative control. (d), Endothelial cells lining a blood vessel adjacent to the tumor foci also stain positive for VEGFR2 (x40).

of the tumor area was around 2.5 mm. Histological examination of H&E-stained brain sections revealed increased mitosis in the tumor cells which demonstrated that ENU1564 cell line was highly invasive.

Histological evaluation of the neoplastic foci. Three weeks after intracranial inoculation with ENU1564 cells the rats were euthanized. Histological evaluation of the brain revealed intracranial neoplasia affecting most frequently the caudate nuclei. Morphologically, clusters of epithelial neoplastic cells resembling the cultured cell line were observed. The tumor foci were devoid of fibrous stroma, and necrosis. Marked gliosis consisting of astrocytes (Fig. 4a) and microglial cells (Fig. 4b) was observed around and inside the neoplastic foci. The data represent three separate experiments with similar results.

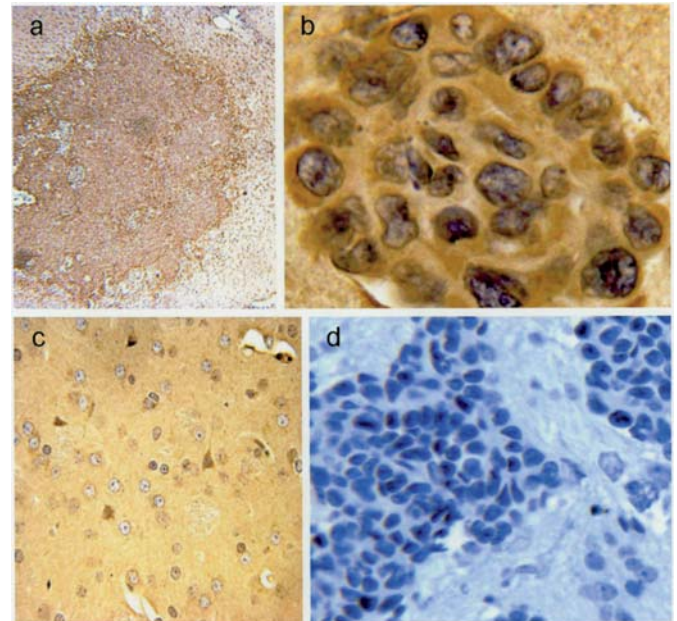


Figure 7. Immunolocalization of VEGF-A in brain tumor foci and surrounding glial cells. (a), Low-power (x4) view of VEGF-A-positive tumor foci. (b), Higher magnification view of tumor cells showing cytoplasmic VEGF-A staining (x40). (c), Positive control (x20) showing VEGF-A labeling of some glial cells. (d), No staining was observed in the negative control (x20).

Immunolocalization of HIF-1 α protein in the tumor foci. Tumor cells respond to low-oxygen conditions via the stabilization and activation of hypoxia-inducible factor-1 α (HIF-1 α), a transcription factor critical for adaptive responses to reduced oxygen. Immunohistochemistry for HIF-1 α was performed in order to demonstrate that hypoxia was localized within the tumor foci. IHC results showed cytoplasmic and nuclear immunolabeling with moderate intensity of the neoplastic cells within the brain tumor foci (Fig. 5a and b). Positive control, represented in Fig. 5c and d, showed that some neurons also had moderate staining in the cytoplasm but not in the nucleus. A negative control is represented in Fig. 5e.

Immunohistochemistry for vascular endothelial growth factor (VEGF-A) and vascular endothelial growth factor receptor

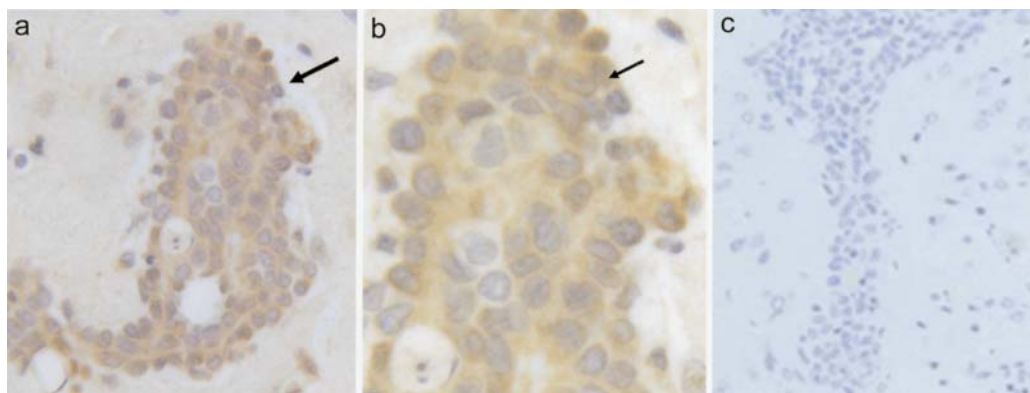


Figure 8. Localization of MMP-9 in the brain metastatic foci. (a), Immunohistochemical staining (brown) of MMP-9 protein in the tumor foci (x20). Note moderate staining in the neurons. (b), Higher magnification view (x40) of the tumor cells showing cytoplasmic MMP-9 staining. Arrows indicate the tumor foci. Negative control for MMP-9 is shown in (c).

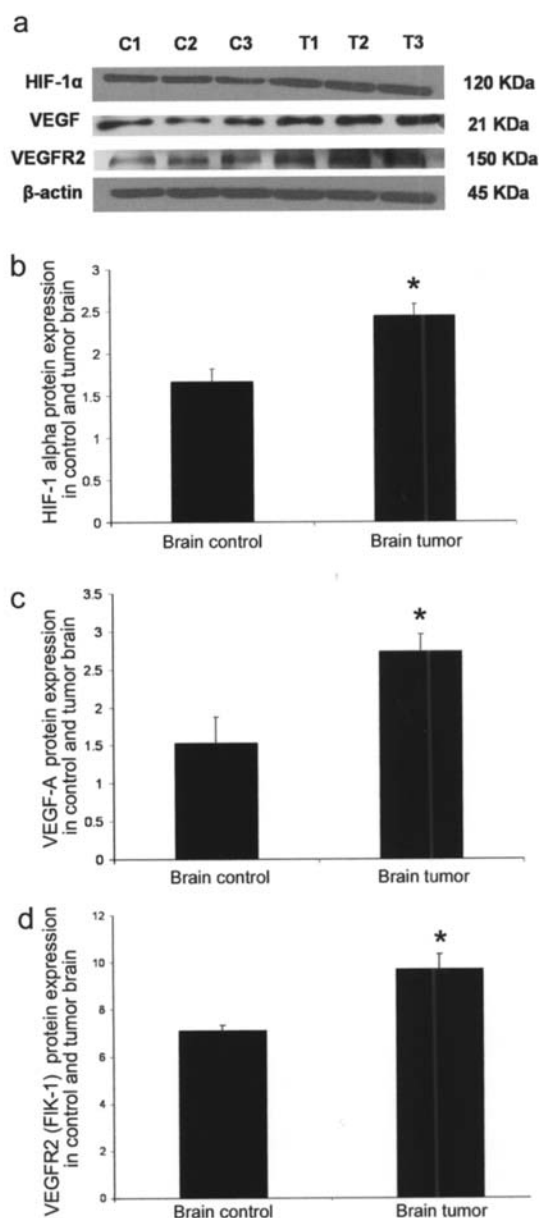


Figure 9. Increased expression of HIF-1 α , VEGF-A, and VEGFR2 (Flk-1) proteins in neoplastic cells. (a), Evaluation of protein expression by Western blotting. The membranes were stripped and re-probed with β -actin antibody to confirm equal loading. (b-d), Densitometric analysis of HIF-1 α , VEGF, and VEGFR2 (Flk-1) protein expression in tumor cells showed significant increases compared with control brain. The results represent the mean \pm standard deviation for three control and three tumor samples. Asterisks indicate statistically significant differences ($P < 0.05$).

VEGFR2 (Flk-1). Further analysis was focused on the VEGF-A and VEGF receptor, VEGFR2 (Flk-1). Immunohistochemical staining for VEGF and VEGFR2 (Flk-1) was performed in order to characterize the expression of these proteins within tumor foci. Previous studies showed that HIF-1 α is the major transcription factor responsible for induction of VEGF production and secretion. IHC staining for VEGFR2 (Flk-1) showed immunolabeling of the neoplastic cells (Fig. 6a and b). Endothelial cells lining blood vessels also show positivity for VEGFR2 (Fig. 6d). No staining was observed in the negative controls (Fig. 6c). VEGF staining was observed in the cytoplasm of the neoplastic cells (Fig. 7a and b). Positive control revealed that some glial cells are also labeled for VEGF-A

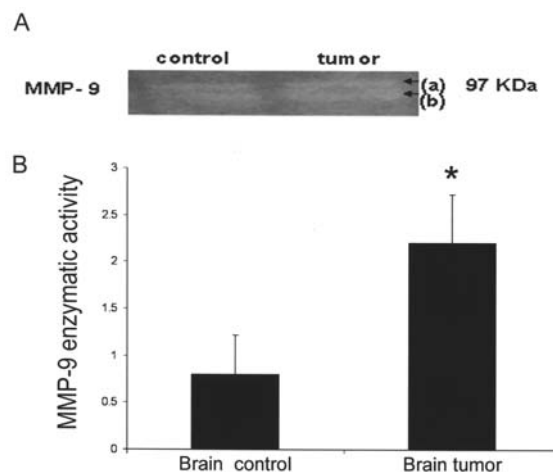


Figure 10. MMP-9 enzymatic activity in tumor foci compared with brain control. (A), Increased MMP-9 enzymatic activity in the tumor foci. The double band at 97 kDa corresponded to the latent form (a) (proenzyme) and active form (b) of MMP-9. (B), Quantitative analysis of MMP-9 was determined by densitometry of the active band (b). Data are represented as mean \pm standard deviation, for three independent experiments and asterisks indicate statistically significant differences ($P < 0.05$).

(Fig. 7c). No staining was observed in the negative controls (Fig. 7d).

Immunohistochemistry for MMP-9 in brain tumor foci. Given the fact that in addition to the upregulation of VEGF hypoxia may be a factor in activation of extracellular matrix degrading proteases we evaluated IHC for MMP-9. Immunohistochemical staining for MMP-9 showed immunolabeling with moderate intensity in the neoplastic cell cytoplasm and faint staining of the glial cells (Fig. 8a and b). Negative control slide is represented in Fig. 8c.

Increased expression of HIF-1 α , VEGF-A and VEGFR2 (Flk-1) proteins in brain tumor foci. To confirm the IHC results on HIF-1 α , VEGF-A and VEGFR2 (Flk-1) we extracted proteins from brain tumor foci and control brain. Evaluation of protein expression by Western blotting revealed that all three proteins were significantly higher in tumor foci compared with control tissue from brains of age-matched-non-inoculated rats (Fig. 9a). Given that HIF-1 α is the major transcription factor responsible for induction of VEGF production and secretion it was important to determine if VEGF was also upregulate in neoplastic cells. VEGFR2 (Flk-1) protein, which is a VEGF receptor was also found to be significantly upregulated in tumor foci. Quantitative analysis (Fig. 9b-d) was determined by densitometry.

Increased MMP-9 activity in brain tumor foci. To confirm the IHC results on MMP-9 protein expression and to evaluate the enzymatic activity of MMP-9 in the brain tumor foci gelatin zymography was performed. The results revealed an increase in enzymatic activity of MMP-9 in brain tumor foci compared with control brain (Fig. 10A). Quantitative analysis determined by densitometry revealed an increase in pro- and active forms of MMP-9. Fig. 10B represents the quantitative analysis of MMP-9 determined by densitometry of the active band (b).

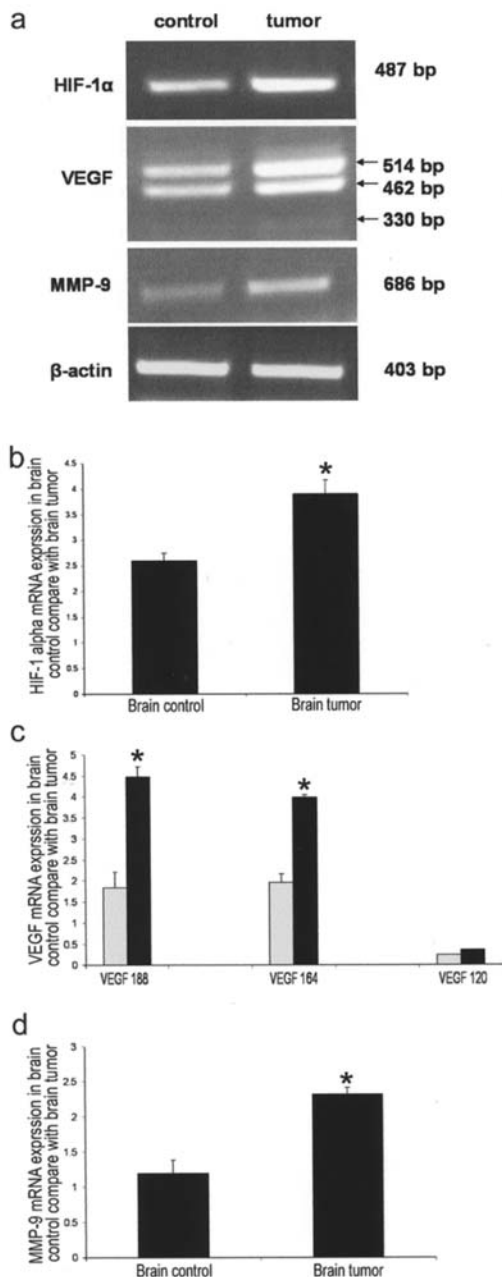


Figure 11. Increased expression of HIF-1 α , VEGF, and MMP-9 mRNA in the rat neoplastic brain foci. (a), Semi-quantitative RT-PCR was used to detect HIF-1 α , VEGF, and MMP-9 and β -actin in total RNAs from normal brain and neoplastic brain foci. β -actin was used as an internal control. For VEGF three alternative splicing variants were identified. A 330-bp product, which is identical to that of the alternative splicing VEGF₁₂₀ isoform. A second 462 bp product, corresponding to the VEGF₁₆₄ isoform, and a third 514-bp product, corresponding to the VEGF₁₈₈ isoform were also detected. VEGF₁₈₈ isoform expression was greater than those of VEGF₁₆₄ and VEGF₁₂₀. (b-d), Quantitative analysis of VEGF, MMP-9, and HIF-1 was determined by densitometry. The results are mean \pm standard deviation from three controls and three tumor samples. *P<0.05.

Increased expression of HIF-1 α , VEGF, and MMP-9 mRNA in the SD rat brain tumor cells. To confirm the IHC and WB results on HIF-1 α , VEGF, and MMP-9 protein expression, we prepared cDNA from dissected tumor sample and performed semi-quantitative RT-PCR analysis. Although this technique is semi-quantitative, our results indicate that there were higher levels of HIF-1 α , VEGF, and MMP-9 mRNA in brain tumor

foci than in normal brain tissues from age-matched non-inoculated rats (Fig. 11a). For VEGF, the RT-PCR from brain control and brain tumor tissues demonstrated three alternative splicing variants: 330, 462 and 514 bp DNA fragments, corresponding to VEGF₁₂₀, VEGF₁₆₄ and VEGF₁₈₈. VEGF₁₈₈ isoform was greater than those of VEGF₁₂₀, and VEGF₁₆₄.

Discussion

In the present study we were able to detect tumor hypoxia in a rat intracranially implanted with a malignant mammary tumor cells by measuring the brain tumor SO₂ through the intact skin and skull using a novel noninvasive spectroscopic photoacoustic tomography technology. Validation of this technology is supported by our molecular biology findings. Detection and measurement of the level of brain blood oxygenation can be used to monitor tumor hypoxia, an important parameter of tumor pathogenesis. We found increased expression of HIF-1 α , VEGF, VEGFR2, and MMP-9 in the brain tumor foci suggesting that these molecules may be induced by tumor hypoxia and may be directly involved in the invasion of the tumor cells into the brain parenchyma. It is known that hypoxia modulates invasion-associated cytokines, such as matrix metalloproteinase, and their inhibitors in tumor and normal cells (35).

Previously, in our laboratory Mendes *et al* using an *in vivo* animal model, showed that MMP-2, -3, and -9 are involved in mammary adenocarcinoma metastasis to the brain (32). The animal model used in those studies was developed in our laboratory (30). The syngeneic animals inoculated with ENU1564 cells via the left ventricle consistently produced brain metastasis. For our study we chose to inoculate the tumor cells (ENU1564) intracranially into the rat forebrain since we were mainly interested in locating tumor implant and detecting tumor hypoxia inside the brain using SPAT, as an assessment of this new technology. The mechanism of tumor invasion resulting from the tumor implant may apply for tumor metastasis because metastasis mediators are involved in both of these processes. Our results showed the presence of tumor hypoxia in the rat brain three weeks post-inoculation.

We used non-inoculated brains of age-matched rats as controls, assuming that differences in HIF-1 α , VEGF, VEGFR2, and MMP-9 would be attributable to the presence of tumors. Our results showed the increased expression of HIF-1 α at both protein and mRNA levels, which is an indicator of the existence of hypoxia in the brain tumor foci. These results were in accordance with previous studies, which showed elevated HIF-1 α expression in a variety of human tumors and pre-neoplastic lesions (20,21). Immunohistochemistry revealed the localization of HIF-1 α protein in the cytoplasm and nucleus of neoplastic cells. Localization of the HIF-1 α in the nucleus is an indication of protein stability in hypoxic conditions which is the major transcription factor responsible for induction of VEGF production but can also activate different genes by binding to their promoter sequences. Hypoxia-induced expression of VEGF has been well established in various types of non-neoplastic and neoplastic cells (36,37).

Considering that previous studies showed that matrix metalloproteinases are important in tumor invasion and metastasis (25,27,32), we focused on MMP-9 expression in brain

tumor foci. Evidence suggested that MMP-9 was associated with intratumoral angiogenesis and with the metastatic process of breast cancer. Our results showed an increased expression of protein and mRNA level of MMP-9 in the brain tumor foci compared with non-inoculated control brain. Gelatin zymography confirmed an increase in gelatinase activity of MMP-9 in tumor brain foci. These results are in accordance with the previous reports correlating MMP-9 activity with invasive and metastatic behavior (38). The upregulation of MMP-9 in brain tumor foci might be directly related to the presence of hypoxia in the brain tumor foci. Interestingly, previous studies showed that besides the upregulation of HIF-1 α in hypoxia other transcription factors such as c-jun/AP-1 (activator protein) are also upregulated (16). Elevation of AP-1 level in hypoxic cells can be one possible mechanism of the MMP-9 upregulation since the promoter of MMP-9 has a site for binding of AP-1 complex.

We analyzed the expression level of protein and mRNA of VEGF and VEGFR2 in brain tumor foci since the mechanism involved in tumor invasion may include hypoxic regulation of cytokine release, and growth factor receptor. In this study, comparison of tumor xenograft and control brains demonstrated that the brain tumor upregulated the expression of VEGF mRNA and protein, which arose as three alternative splicing variants VEGF₁₂₀, VEGF₁₆₄ and VEGF₁₈₈. The genetic studies showed that the VEGF₁₂₀ isoform alone is able to initiate, but not complete, the angiogenic programme (39). Although the target of VEGF was thought to be restricted to endothelial cells, more and more evidence has indicated that non-endothelial cells can be VEGF targets by expressing VEGF receptors (13). The production and upregulation of VEGF in brain tumor foci is important for tumor vascularization and may confer proteolytic activity to the neoplastic cells by induction of MMP-9. Our results showed that VEGFR2 protein was up-regulated in brain tumor foci compared with brain control (Fig. 9a). VEGFR2 is considered to be the main mitogenic signaling receptor for VEGF (19). Skobe *et al* demonstrated the role of VEGFR2 for the invasive growth of skin squamous cell carcinoma cells (40). Recently, Noda *et al* demonstrated the hypoxic upregulation of VEGF and VEGFR2 and their involvement in hypoxia-induced MT1-MMP expression in retinal glial cells. This upregulation was abrogated in the presence of SU1498, a selective inhibitor of VEGFR2 or by using a neutralizing anti-VEGF antibody (41). The upregulation of VEGF, VEGFR2 and MMP-9 might be a consequence of decreased tissue oxygen concentration which leads to up-regulation of HIF-1 α . Direct or indirect interaction of both transcription factors c-jun/AP-1 and HIF-1 α is a suggested mechanism for regulation of at least some of the known hypoxia-inducible genes. Upregulation of all these factors under hypoxic conditions enables the cells to survive reduced tissue oxygen concentration by promoting angiogenesis and tumor metastasis.

Because evidence suggested that astrocytes and/or glial cells may have a role in tumor invasion (32) we analyzed how these cell types reacted in a tumor-bearing brain. Prior studies showed that astrocytes are thought to play a role in MMP-9 activation and expression (42). Immunohistochemical staining using GFAP antibody (glial fibrillary acidic protein) demonstrated marked astrocytic proliferation around neoplastic foci

(Fig. 4a). Astrocytes, which populated brain parenchyma, synthesized a host of biological proteins including TGF- β , TNF- α , interferon- γ , IL-1, IL-3, IL-6, and other cytokines which may be very important for tumor invasion (42). Studies showed that brain metastatic and parental cancer cell line co-cultured with astrocytes or cell culture supernatants of astrocytes, exhibited increased adherence to astrocytes and grew better in response to the conditioned media (43). Microglial reactivity around and inside the tumor foci was also confirmed (Fig. 4b). The presence of reactive glial cells around tumor cells in the brain suggests the possibility that these cell types could be interacting. Further studies are needed in order to characterize the role of those cells in tumor progression into the brain parenchyma.

Tumor oxygen status appears to be strongly associated with tumor growth, malignant progression, and resistance to various therapies (1). Among the genes upregulated in hypoxia, those involved in angiogenesis and degradation of extracellular matrix appears to be very important in malignant progression (12). Tumor oxygen status may also be important in the assessment of the efficacy of agents classified as antiangiogenic compounds, which target tumor vasculature (1). Therapy with antiangiogenic compounds may be more important than those which cause direct cytotoxicity to malignant cells. Detection of tumor hypoxia can be used as a prognostic tool and for developing and evaluating patient specific treatment modalities for many types of cancer. In 2004, Evans *et al* showed that the presence of more severe hypoxia in glial tumors correlated with a more aggressive clinical behavior (44). Also, the presence of hypoxia in locally cured high-grade sarcomas was associated with a greater likelihood of metastasis and death (45).

This study shows that SPAT would be an important tool for noninvasive detection of intracranial tumors. Moreover, SPAT would be useful for monitoring the development of hypoxia, which may have an important role in determining the timing and type of therapy. SPAT is also a promising imaging modality for the study of the functional and structural organization of the brain. In combination with reporter genes, SPAT offers promise for imaging pathological processes at molecular levels, and monitoring the delivery of vectors to specific cells by gene therapy.

Acknowledgements

We are grateful to Dr G. Bratton for critical reading of the manuscript. This work was supported by a National Institute of Health grant (no. R01-N5046214-01).

References

1. Dewhirst MW, Klitzman B, Braun RD, Brizel DM, Haroon ZA and Secomb TW: Review of methods used to study oxygen transport at the microcirculatory level. *Int J Cancer* 90: 237-255, 2000.
2. Howe FA, Robinson SP and Griffiths JR: Modification of tumor perfusion and oxygenation monitored by gradient recalled echo MRI and 31P MRS. *NMR Biomed* 208-216, 1999.
3. Wilson D and Cerniglia G: Oxygenation of tumors as evaluated by phosphorescence imaging. *Adv Exp Med Biol* 345: 539-547, 1994.
4. Helmlinger G, Yuan F, Dellian M and Jain RK: Interstitial pH and pO₂ gradients in solid tumors *in vivo*: high-resolution measurements reveal a lack of correlation. *Nat Med* 3: 177-182, 1997.

5. Dewhirst MW, Ong ET, Braun RD, *et al*: Quantification of longitudinal tissue pO₂ gradients in window chamber tumors: impact on tumor hypoxia. *Br J Cancer* 79: 1717-1722, 1999.
6. Mueller KW, Vaupel P, Manz R and Schmidseider R: Intracapillary oxyhemoglobin saturation of malignant tumors in humans. *Int J Radiat Oncol Biol Phys* 7: 1397-1404, 1981.
7. Rasey JS, Koh WJ, Evans ML, *et al*: Quantifying regional hypoxia in human tumors with positron emission tomography of [¹⁸F]fluoromisonidazole: a pretherapy study of 37 patients. *Int J Radiat Oncol Biol Phys* 36: 417-428, 1996.
8. Chapman JD, Engelhardt EL, Stobbe CC, Schneider RF and Hanks GE: Measuring hypoxia and predicting tumor radioresistance with nuclear medicine assays. *Radiother Oncol* 46: 229-237, 1998.
9. Evans S, Jenkins W, Joiner B, Lord E and Koch C: 2-Nitroimidazole (EF5) binding predicts radiation resistance in individual 9L s.c. tumors. *Cancer Res* 56: 405-411, 1996.
10. Ku G, Wang X, Xie X, Stoica G and Wang LV: Imaging of tumor angiogenesis in rat brains *in vivo* by Photoacoustic tomography. *Appl Optics* 44: 770-775, 2005.
11. Wang X, Pang Y, Ku G, Xie X, Stoica G and Wang LV: Non-invasive laser-induced photoacoustic tomography for structural and functional imaging of the brain *in vivo*. *Nat Biotechnol* 21: 803-806, 2003.
12. Risau W: Mechanisms of angiogenesis. *Nature* 386: 671-674, 1997.
13. Carmeliet P and Jain RK: Angiogenesis in cancer and other diseases. *Nature* 407: 249-257, 2000.
14. Wang H and Keiser JA: Vascular endothelial growth factor upregulates the expression of matrix metalloproteinases in vascular smooth muscle cells: role of flt-1. *Circ Res* 83: 832-840, 1998.
15. Vaupel P and Hockel M: Tumor oxygenation and its relevance to tumor physiology and treatment. *Adv Exp Med Biol* 510: 45-49, 2003.
16. Kunz M and Saleh MI: Molecular response to hypoxia in tumor cells. *Mol Cancer* 2: 1457-1470, 2003.
17. Semenza GL: HIF-1 and tumor progression: pathophysiology and therapeutics. *Trends Mol Med* 8: S62-S67, 2002.
18. Semenza GL, Jiang BH, Leung SW, *et al*: Hypoxia response elements in the aldolase A, enolase 1, and lactate dehydrogenase A gene promoters contain essential binding sites for hypoxia-inducible factor 1. *J Biol Chem* 271: 32529-32537, 1996.
19. Kaur B, Khwaja FW, Severson EA, Matheny SL, Brat DJ and Meir EV: Hypoxia and hypoxia-inducible-factor pathway in glioma growth and angiogenesis. *Neuro-oncology* 7: 134-153, 2005.
20. Zhong H, De Marzo AM, Laughner E, *et al*: Overexpression of hypoxia-inducible factor 1alpha in common human cancers and their metastases. *Cancer Res* 59: 5830-5835, 1999.
21. Talks KL, Turley H, Gatter KC, *et al*: The expression and distribution of the hypoxia-inducible factors HIF-1alpha and HIF-2alpha in normal human tissues, cancers, and tumor-associated macrophages. *Am J Pathol* 157: 411-421, 2000.
22. Cairns RA, Kalliomaki T and Hill RP: Acute (cyclic) hypoxia enhances spontaneous metastasis of KHT murine tumors. *Cancer Res* 61: 8903-8908, 2001.
23. Rofstad EK: Microenvironment-induced cancer metastasis. *Int J Radiat Biol* 76: 589-605, 2000.
24. Leppa S, Saarto T, Vehmanen L, Blomqvist C and Elomaa I: A high serum matrix metalloproteinase-2 level is associated with an adverse prognosis in node-positive breast carcinoma. *Clin Cancer Res* 10: 1057-1063, 2004.
25. Nabeshima K, Inoue T, Shimao Y, Shimao Y and Sabeshima T: Matrix metalloproteinases in tumor invasion: role for cell migration. *Pathol Int* 52: 255-264, 2002.
26. Chang C and Werb Z: The many faces of metalloproteases: cell growth, invasion, angiogenesis and metastasis. *Trends Cell Biol* 3: 11-18, 2001.
27. Kato Y, Lambert AC, Colige AC, *et al*: Acidic extracellular pH induces matrix metalloproteinase-9 expression in mouse metastatic melanoma cells through the phospholipase D-mitogen-activated protein kinase signaling. *J Biol Chem* 280: 109-123, 2005.
28. Ikeda E, Achen MG, Breier G and Risau W: Hypoxia-induced transcriptional activation and increased mRNA stability of vascular endothelial growth factor in C6 glioma cells. *J Biol Chem* 270: 19761-19766, 1995.
29. Xu L, Fukumura D and Jain RK: Acidic extracellular pH induces vascular endothelial growth factor (VEGF) in human glioblastoma cells via ERK 1/2 MAPK signaling pathway. *J Biol Chem* 277: 11368-11374, 2002.
30. Hall DG and Stoica G: Characterization of brain and bone-metastasing clones selected from an ethylnitrosourea-induced rat mammary carcinoma. *Clin Exp Metastasis* 12: 283-295, 1994.
31. Lee P, Hwang J, Murphy G and Margot M: Functional significance of MMP-9 in tumor necrosis factor-induced proliferation and branching morphogenesis of mammary epithelial cells. *Endocrinology* 141: 3764-3773, 2000.
32. Mendes O, Kim HT and Stoica G: Expression of MMP-2, MMP-9 and MMP-3 in breast cancer brain metastasis in a rat model. *Clin Exp Metastasis* 22: 237-246, 2005.
33. Turcotte S, Desrosiers RR and Beliveau R: HIF-1 α mRNA and protein upregulation involves Rho GTPase expression during hypoxia in renal cell carcinoma. *J Cell Sci* 116: 2247-2260, 2003.
34. Xu M, Xu Y and Wang LH: Time-domain reconstruction algorithms and numerical simulations for thermoacoustic tomography in various geometries. *IEEE Trans Biomed Eng* 50: 1086-1099, 2003.
35. Ben YY, Lahat N, Shapiro S, *et al*: Regulation of endothelial matrix metalloproteinase-2 by hypoxia/reoxygenation. *Circ Res* 90: 784-791, 2002.
36. Kondo S, Kubota S, Shimo T, *et al*: Connective tissue growth factor increased by hypoxia may initiate angiogenesis in collaboration with matrix metalloproteinases. *Carcinogenesis* 23: 769-776, 2002.
37. Semeza GL: Angiogenesis in ischemic and neoplastic disorder. *Annu Rev Med* 54: 17-28, 2003.
38. Yu AQ and Stamenkovic I: Localization of matrix metalloproteinase-9 to the cell surface provides a mechanism for CD44-mediated invasion. *Gene Dev* 13: 35-48, 1999.
39. Carmeliet P: Impaired myocardial angiogenesis and ischemic cardiomyopathy in mice lacking the vascular endothelial growth factor isoforms VEGF164 and VEGF188. *Nat Med* 5: 495-502, 1995.
40. Skobe M, Rockwell P, Goldstein N, Vosseler S and Fusenig NE: Halting angiogenesis suppresses carcinoma cell invasion. *Nat Med* 3: 1222-1227, 1997.
41. Noda K, Ishida S, Shinoda H, *et al*: Hypoxia induces the expression of membrane-type 1 matrix metalloproteinase in retinal glial cells. *Invest Ophthalmol Vis Sci* 46: 3817-3824, 2005.
42. Arai K, Lee S and Loo EH: Essential role for ERK mitogen-activated protein kinase in matrix metalloproteinase-9 regulation in rat cortical astrocytes. *Glia* 43: 254-264, 2003.
43. Sierra A, Price J, Garcia RM, Mendez O, Lopez L and Fabra A: Astrocyte derived cytokines contribute to the metastatic brain specificity of breast cancer cells. *Lab Invest* 77: 357-368, 1997.
44. Evans SM, Judy KD and Dunphy I: Hypoxia is important in the biology and aggression of human glial brain tumors. *Clin Cancer Res* 10: 8177-8184, 2004.
45. Brizel DM, Scully SP, Harrelson JM, *et al*: Tumor oxygenation predicts for the likelihood of distant metastases in human soft tissue sarcoma. *Cancer Res* 56: 941-943, 1996.